Available online at www.sciencedirect.com
SCIENCE DIRECT
Tetrahedron
Tetrahedron 62 (2006) 3721–3731

Ab initio study of molecular structures and excited states in anthocyanidins

Ken Sakata,* Norio Saito and Toshio Honda

Faculty of Pharmaceutical Sciences, Hoshi University, Ebara 2-4-41, Shinagawa, Tokyo 142-8501, Japan

Received 7 December 2005; accepted 16 January 2006

Available online 28 February 2006

Abstract—The structural and electronic characters of four types of hydroxyl group-substituted anthocyanidins (pelargonidin, cyanidin, delphinidin, and aurantinidin) were examined using quantum chemical calculations. For these cationic molecules, both the planar and non-planar structures in the electronic ground state were determined at the B3LYP/D95 level of theory. We revealed that the planar structure is slightly more stable than the non-planar structure for each molecule. For the optimized planar structures, single excitation–configuration interaction (SE–CI) based on the restricted Hartree–Fock (RHF) wave function was evaluated and the electronic character in the low-excited states was discussed in terms of the MO theory. Symmetry adapted cluster (SAC)/SAC-CI calculations were also carried out to estimate the excitation energies precisely. The results showed that hydroxylation of the phenyl group causes a change in the excitation energies without taking the solvent effects into account. The results are in agreement with spectral experiments and previous MO calculations.

1. Introduction

Anthocyanidins are polyoxygenated derivatives of 2-phenylbenzopyrylium cation, which consist of three six-membered rings, A-, B-, and C-rings, as shown in Figure 1. Glycosylated anthocyanidins, which are called anthocyanins, are most important floral pigments and give rise to a wide range of flower colors from orange to blue. The origin of the variation in flower colors conferred by anthocyanin pigments has been an interesting subject of study since the early twentieth century[1–7] and five main subjects have been discussed to understand the phenomenon to date:

(1) *The structures of anthocyanidins*. Firstly anthocyanidins play a most important role producing flower colors as the chromophore, and three anthocyanidins (pelargonidin, cyanidin, and delphinidin) are well known to be principal and basic skeletons of flower color pigments. The visible absorption spectra of these molecules differ in proportion to the number of hydroxyl groups in the B-rings.[1,2,8,9] Methylation and glycosydation of the hydroxyl groups also affects rather slightly the absorption spectra.[1,2] (2) *Tautomerism*. Secondly anthocyanidins show prototropic equilibria depending on the pH of the solution and change their colors like litmus.[5,6] In strong acid solution, the cationic forms are dominant. At pH 3.0–7.0, neutral quinonoidal forms become predominant while anionic forms exist mainly in alkaline solution. In neutralized aqueous solution, a pseudo-base form is also produced when the hydration reaction occurs. These respective forms have

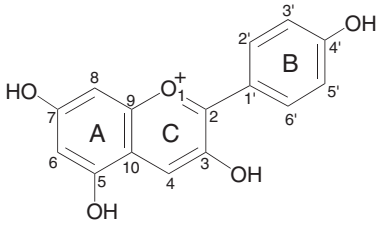

	$C_{3'}$	$C_{5'}$	C_6	
	–H	–H	–H	**1** (pelargonidin)
	–OH	–H	–H	**2** (cyanidin)
	–OH	–OH	–H	**3** (delphinidin)
	–H	–H	–OH	**4** (aurantinidin)

Figure 1. Structure and atom numbering of the anthocyanidins examined.

Keywords: Anthocyanidin; Quantum chemical calculations.
* Corresponding author. Tel./fax: +81 3 5498 5078; e-mail: sakata@hoshi.ac.jp

0040–4020/$ - see front matter © 2006 Elsevier Ltd. All rights reserved.
doi:10.1016/j.tet.2006.01.081

different spectral properties and give specific colors. (3) *Self-association*. It has been thought that the self-association of anthocyanin prevents the hydration reaction in the case of a high-concentration solution and keeps its color stability.[10] (4) *Intra- and inter- molecular copigmentation*. Robinson and Robinson[10,11] showed that anthocyanins make certain complexes (copigmentation) with copigments such as flavone, flavonol, and tannin by intermolecular interaction (intermolecular copigment). The copigmentation protects the anthocyanidin molecule from the hydration reaction, and also controls somewhat its color in response to its tightness. Later, Saito et al.[12,13] found that anthocyanins also make the intramolecular copigments with the aromatic organic acid in their glycosides. (5) *Metal-complex effect*. Shibata et al.[14] suggested that anthocyanin gives a stable blue color upon the formation of a metal-complex. Their metal-complex theory has been the subject of much controversy and the crystal structures of the metal-complex have recently been determined.[15,16]

These factors are considered to contribute to the variation in the structural stabilities and electronic structures of anthocyanins, and therefore flowers show various colors.

To understand the mechanism of the flower color variation, the more accurate information on the chemical nature of anthocyanidins, particularly the electronic structure is needed because all of the above factors are believed to reflect chemical interactions. Some theoretical studies on the stable structures and excitation energies of anthocyanidins have already been reported.[17–28] Pauling[17] applied the resonance concept to anthocyanidins and indicated a close relation between the absorption spectra and π-electron structures. Bendz et al.[18] calculated the π-electron structures of a series of flavylium compounds using the semi-empirical PPP method and discussed electronic character in the ground state in terms of atomic charges and bond orders. Song et al.[19,20] investigated the absorption spectra and electronic structures of anthocyanidin cationic molecules using simple Hückel and PPP methods.

Recently, Rastelli et al.[21] investigated the stabilities of tautomers in three anthocyanidins (apigeninidin, pelargonidin, and cyanidin) using the semi-empirical MO method based on the AM1 Hamiltonian. They found that the cationic, neutral, and anionic forms each show a stable structure and concluded that the important factors in determining these stabilities are both the extent of π-electron delocalization and the classical resonance structures. Pereira et al.[22] examined the flavylium cation and its hydroxylated derivatives using the semi-empirical AM1 and ab initio Hartree–Fock methods and discussed these structures, charge distributions, bond orders, and MOs. They also investigated the electronic structures of hydroxylated derivatives in the B-ring and indicated that hydroxy substitutions in the B-ring, except for the C3′-position, cause an increase in resonance through the C2–C1′ bond.[23] Moreover, they examined the electronic excited states in some anthocyanidins using the semi-empirical INDO1/S and AM1 methods.[24] They concluded that hydroxylation in the B-ring causes a bathochromic shift in the absorption spectra.

Torskangerpoll et al.[25] estimated the excitation energies of 18 derivatives of hydroxyl-substituted anthocyanidins by the semi-empirical ZINDO/S and ab initio CIS methods. Moreover, they applied the multivariate regression model to the quantitative estimation of the visible absorption maxima λ_{max} by using theoretical and positional parameters. Merlin et al.[26] performed a molecular mechanics (MM) study to better understand the results of the resonance Raman spectra of anthocyanidins. Moreover, they clarified the possibility of the intramolecular copigmentation of the hemiacetal form in delphinidin 3-gentiobioside with the hydrogen-bond between the OH of glycoside and the OH of hemiacetal using both the AM1 MO and MM methods.[27,28]

At the present, we investigate theoretically the mechanism of flower color variations in anthocyanins by considering the above five factors. As a first step in a series of theoretical studies on anthocyanin, the structural stabilities and electronic structures of four anthocyanidin molecules (Fig. 1) (pelargonidin, cyanidin, delphinidin, and aurantinidin) are investigated using quantum chemical calculations. To the best of our knowledge, there has been no previous study on anthocyanidin molecules using high-level ab initio calculations. Thus, we examine the structural and electronic characteristics in the solvent-free cationic forms of these anthocyanidins. As shown in Table 1, the absorption maxima λ_{max} of these molecules in acidic media become bathochromic in proportion to hydroxylation in the B-ring, while a hypsochromic shift occurs by hydroxyl substitution at the 6-position in the A-ring. These phenomena are considered to reflect differences in the effects of the position of hydroxylation on the electronic structure.

Table 1. Absorption maxima λ_{max} of anthocyanidins in the visible region[a]

Anthocyanidin	λ_{max} (nm)	
	Methanol–HCl	Ethanol–HCl
Pelargonidin	520	530
Cyanidin	535	545
Delphinidin	546	557
Aurantinidin	499	—

[a] Refs. 1,9.

In the present study, we examined the stable structures of these cationic molecules by the density functional theory (DFT). As shown in Figure 2, we calculated two types of geometries, the planar structure and the non-planar structure, according to the orientation of the 3-OH group. Next, we performed single excitation–configuration interaction (SE–CI) calculations based on the restricted Hartree–Fock (RHF) wave functions to examine the electronic characters in the low-excited states from the perspective of the MO theory. Finally, we carried out symmetry adapted cluster (SAC)/SAC-CI calculations. As a result, we clarified the variation in the lowest excitation energy due to the hydroxy substitution in isolated cationic molecules.

2. Computational details

The stable structures in the ground state were optimized by the DFT using Becke's three-parameter hybrid method[29] with the Lee, Yang, and Parr correlation functional[30]

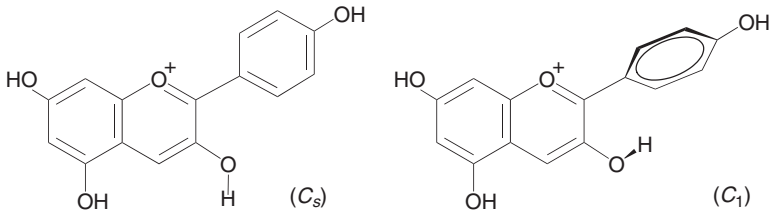

1a **1b**

Figure 2. Planar (**1a**) and non-planar (**1b**) structures of pelargonidin.

(B3LYP). Dunning's (9s5p/4s)/[4s2p/2s] contracted basis set (D95) was used for the Gaussian basis functions.[31,32] For both the ***n*a** and ***n*b** ($n=1$–4) structures, which differ in the orientation of the 3-hydroxyl group, we adopted the most stable structures within the optimized local minima, which varied in the orientation of the hydroxyl groups, except for 3-OH. The theoretical harmonic vibrational frequencies were obtained from the analytical second derivatives to verify that the equilibrium structures are true minima.

To examine the electronic character in the low-excited states in planar structures ***n*a** ($n=1$–4), SE–CI calculations were carried out using the RHF orbitals as reference orbitals. In the SE–CI calculations, the 1s orbitals of C and O atoms and their antibonding counterparts at the top of the unoccupied space were treated as frozen cores. The basis sets used in the SE–CI calculations were the D95 basis set and D95 plus d-type polarization functions to C ($\alpha=0.75$) and O ($\alpha=0.85$) atoms (D95(d)).[32]

Finally, the ground and singlet A′ excited states at planar structures ***n*a** ($n=1$–4) were calculated by the SAC/SAC-CI SD-*R* method.[33–36] In the SAC/SAC-CI calculations, the D95 basis set was employed and the RHF orbitals were used as the reference orbitals. All valence orbitals were included in the active space and the space of the frozen cores was similar to those in the SE–CI calculations. All single excitations and selected double excitations are included in the linked term. Perturbation selection[37,38] was performed with energy thresholds of 1×10^{-6} a.u. for the ground state and 1×10^{-7} a.u. for the excited states. The resultant dimensions for the SAC/SAC-CI calculations are shown in Table 2. We calculated nine excited A′ states although only the lowest three excited states are shown in the results. For the ground state, the unlinked terms are described as the products of the important linked terms for which the SD–CI coefficients were greater than 0.005. For the singlet excited states, all *S* operators and important *R* operators for which the SD–CI coefficients are greater than 0.05 were included in the unlinked term.

Table 2. Dimensions of the linked terms for SAC/SAC-CI calculations

	Reference state	Before selection	After selection
1a			
Ground state (SAC) A′	1	11,873,732	328,975
Excited state (SAC-CI) A′	9	11,873,732	572,384
2a			
Ground state (SAC) A′	1	14,326,280	353,410
Excited state (SAC-CI) A′	9	14,326,280	597,062
3a			
Ground state (SAC) A′	1	17,135,580	363,787
Excited state (SAC-CI) A′	9	17,135,580	664,113
4a			
Ground state (SAC) A′	1	14,326,280	344,273
Excited state (SAC-CI) A′	9	14,326,280	625,072

All quantum chemical calculations were carried out with the Gaussian03[39] and GAMESS[40] program packages.

3. Results and discussion

3.1. Stable structures

Both the planar structures ***n*a** and non-planar structures ***n*b** ($n=1$–4) are represented in Figure 3. Figure 3 also shows the Mulliken atomic charges[41] based on the Kohn–Sham orbitals. The relative energy difference between ***n*a** and ***n*b**, ΔE, is shown in Table 3. The Mayer bond order[42] and dipole moments are shown in Table 4.

For all molecules, both the planar ***n*a** and non-planar ***n*b** structures were obtained at the B3LYP/D95 level of theory. All of the frequencies for these geometries have real numbers, so that these structures were confirmed to be minima. For pelargonidin, the structure **1a** is more stable than **1b** by 3.4 kcal/mol at the B3LYP/D95(+ZPE) level, as shown in Table 3. For cyanidin and delphinidin, the planar structures, **2a** and **3a**, are more stable than **2b** and **3b** by 3.0 and 3.4 kcal/mol, respectively. Structure **4a** is also more stable than **4b** by 3.6 kcal/mol. Thus, for all of these molecules, the planar structures are more stable than the non-planar structures. Although the trend in the relative stabilities did not change, the ΔE values at the B3LYP/D95(d)//B3LYP/D95(+ZPE) level are smaller than those at the B3LYP/D95(+ZPE) level. Therefore, there is a slight possibility for the existence of non-planar structures in which the B-ring is distorted in response to the orientation of the 3-OH, although these structures are more unstable than the planar structures. The structural variations according to the orientation of the 3-substituent group become important in the case of 3-glucoside forms.

X-ray crystal analyses of pelargonidin and cyanidin bromide monohydrides have been reported.[43,44] Based on both the orientation of 3-OH and the dihedral angle (ϕ(O1C2C1′C2′)=3.8° for pelargonidin and 10.1° for cyanidin), the structures of pelargonidin and cyanidin in the crystals may correspond to structures **1a** and **2a** rather than **1b** and **2b**. The bond lengths calculated at the B3LYP/D95 level are 0.01–0.03 Å longer than those obtained by

the X-ray crystal analysis, except for the C1′–C2 bond. For the C1′–C2 bond, the bond lengths are 1.439 Å in **1a** and 1.443 Å in **2a**, which are shorter than those in the crystals by 0.019 Å in **1a** and 0.010 Å in **2a**. The orientations of the other hydroxyl groups except for 3-OH in **1a** and **2a** are different from those in the crystals. This is because the crystal structures depend on orientations, which are favorable for the formation of the hydrogen-bond network for crystal stability. The calculated planar structure, which corresponds to the orientations of all hydroxyl groups in the crystal structure is more unstable than **2a** by 6.9 kcal/mol.

MM and semi-empirical calculations have also been reported for the anthocyanidin structures[21,26] although these previous studies did not discuss the existence of some conformers according to orientation of the 3-OH group. The results of the MM calculation by Merlin et al.[26] were compared to the present results. The orientation of 3-OH is in agreement with that in **2a**. The bond lengths and orientations of the other OH groups are also consistent with those in planar structure **2a**. However, the dihedral angle, ϕ(O1C2C1′C2′), has been reported to be 28.6°, which is close to that in structure **2b**. Meanwhile, Rastelli et al.[21] reported that the C1′–C2 bond length is 1.433 Å and the dihedral angle ϕ(O1C2C1′C2′) is 0.3° in pelargonidin at the semi-empirical AM1 level. In cyanidin, the C1′–C2 bond length is 1.440 Å, which corresponds to that in planar structure **2a** while the dihedral angle ϕ(O1C2C1′C2′) is 19.0°, which corresponds to that in **2b**.

Next, we discuss the differences between two types of structures, ***n*a** and ***n*b**, in the same molecule. For the C1′–C2 bond, which connects the B-ring to the C-ring, the bond length in **1a** is 1.439 Å, which is shorter than that in **1b** (1.448 Å). In response to the bond length, the bond orders are also different. As shown in Table 4, the bond order of this bond in **1a** is 1.140, while that in **1b** is 1.043. Based on both the bond length and the bond order, it is shown that the bond in **1a** is stronger than that in **1b**. A difference in the bond strength is also seen for the other molecules. This corresponds to the fact that delocalization of the π-bond between two planes (the benzopyrylium ring and the B-ring) is not expected in the non-planar structure. Thus, the bond in **1b** is considered to be a single bond while that in **1a**

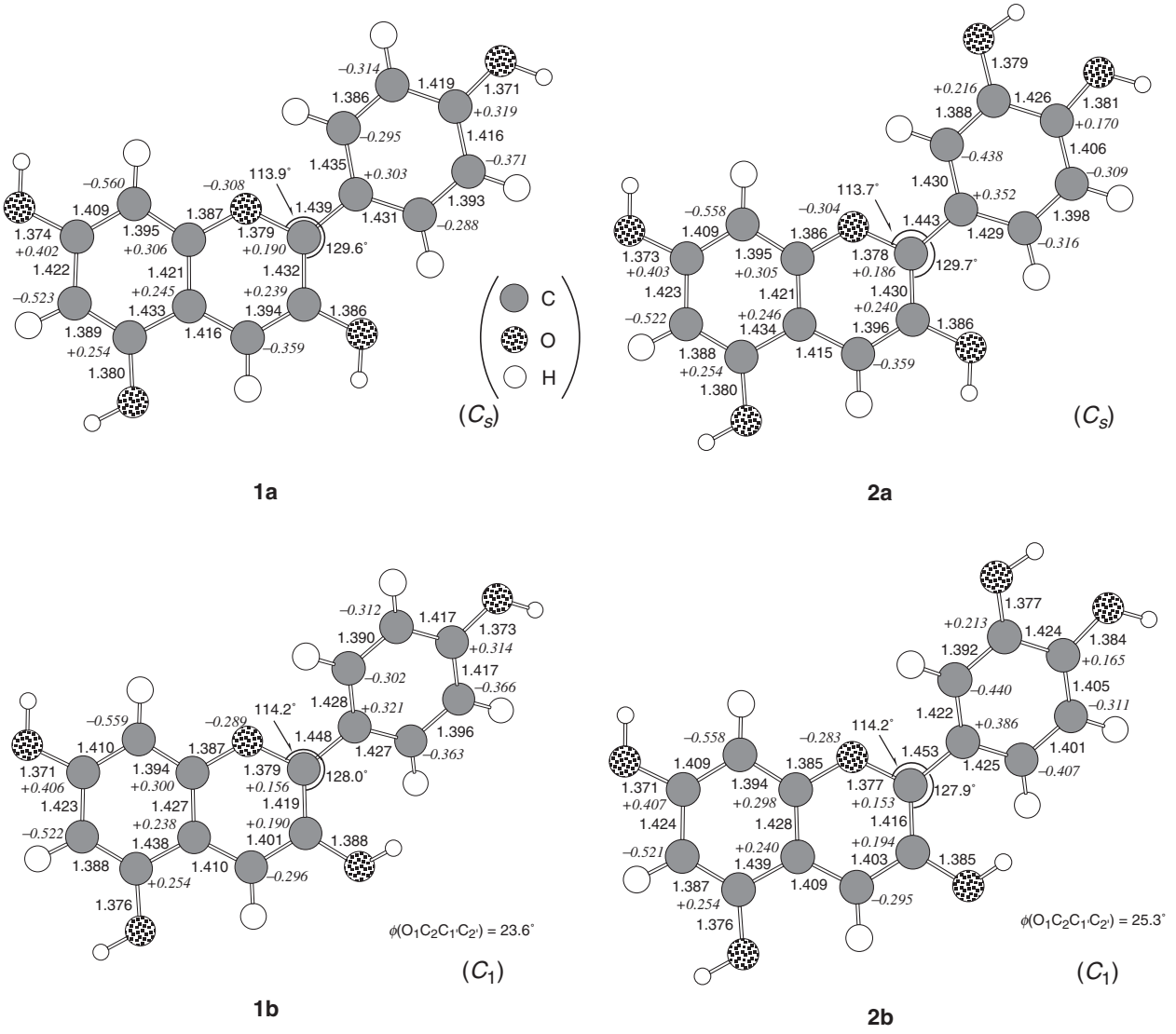

Figure 3. Optimized geometries at the B3LYP/D95 level. Bond length is in Å and bond angle is in degrees. The Mulliken atomic charges are in italics.

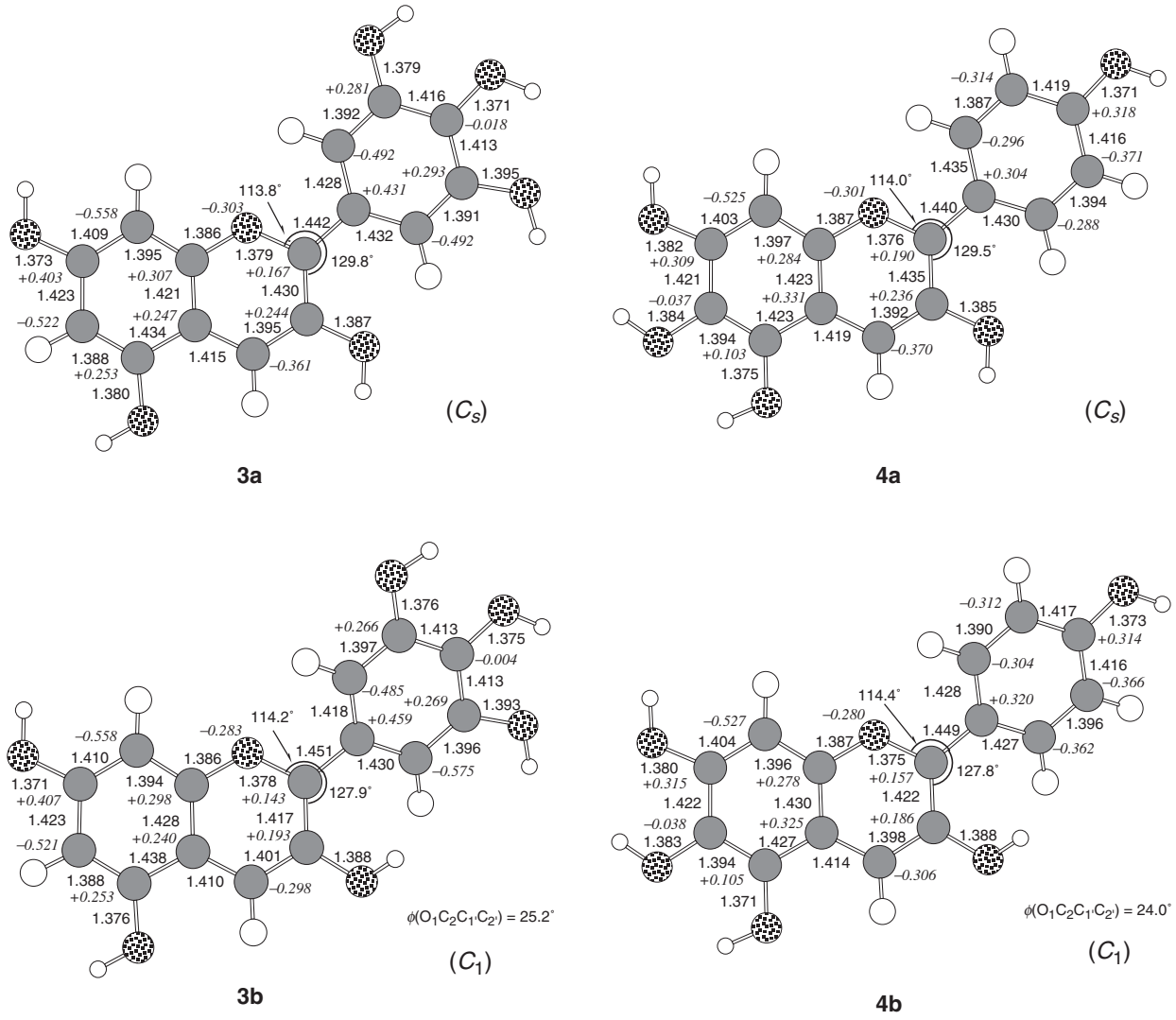

Figure 3 (*continued*)

possesses a slight π-bond character. Structural differences are also seen in the benzopyrylium part (A- and C-rings). The C2–C3 and C4–C10 bonds in planar structure ***n*a** are longer than those in ***n*b**, while the C3–C4, C9–C10, and C5–C10 bonds are shorter. The magnitudes of the bond orders in the C-ring correspond to the bond length. The bond orders of the C3–C4, C9–C10, and C5–C10 bonds in ***n*a** are larger than those in ***n*b** while the bond orders of the O1–C2, C2–C3 and C4–C10 bonds at ***n*a** are smaller. The atomic charges at the C-ring are also mostly different. The atomic charges at the O1 and C4 atoms in ***n*a** are more negative than those in ***n*b**. On the other hand, the charges at the C2 and C3 atoms in ***n*a** are more positive than those in ***n*b**. The C4 atomic charge has the greatest change. The π-bond character in the C2–C1′ bond is not seen in the non-planar structure ***n*b**, so that the distributions of the π-electrons in the C-ring in ***n*b** are different from those in ***n*a**.

Table 3. Relative energies Δ*E* (kcal/mol)

	B3LYP/D95	B3LYP/D95 (+ZPE)	B3LYP/D95(d)// B3LYP/D95(+ZPE)
1a	0.0	0.0	0.0
1b	3.7	3.4	1.8
2a	0.0	0.0	0.0
2b	3.2	3.0	1.3
3a	0.0	0.0	0.0
3b	3.7	3.4	1.5
4a	0.0	0.0	0.0
4b	3.9	3.6	1.9

We now discuss the structural variations due to substitutions of the hydroxyl group. In both the planar and non-planar structures, the C1′–C2 bond lengths in cyanidin are longer than those in pelargonidin, while the bond lengths in delphinidin are slightly shorter than those in cyanidin. The bond order of this bond decreases with successive hydroxyl substitutions. At the same time, the atomic charge at the C1′ atom becomes positive while that at the C2 atom becomes negative. In the case of pelargonidin, the C1′–C2 bond is strengthened by the *para*-OH group in the B-ring. On the other hand, the bond order analysis shows that introduction of the *meta*-OH groups makes the bond weaker. In aurantinidin, a definite change is not observed in comparison with pelargonidin. These variations in bond strength are also observed in the torsional vibrational mode of the

Table 4. Mayer bond orders *I* and dipole moments μ at the B3LYP/D95 level

	1a	**1b**	**2a**	**2b**	**3a**	**3b**	**4a**	**4b**
I								
O1–C2	1.065	1.085	1.069	1.089	1.077	1.094	1.076	1.098
C2–C3	1.268	1.303	1.281	1.315	1.278	1.312	1.260	1.291
C3–C4	1.390	1.336	1.381	1.323	1.386	1.332	1.406	1.355
C4–C10	1.172	1.221	1.179	1.232	1.177	1.227	1.107	1.155
C9–C10	1.321	1.286	1.317	1.280	1.317	1.282	1.286	1.245
C5–C10	1.164	1.155	1.161	1.151	1.163	1.154	1.167	1.161
C2–C1′	1.140	1.043	1.108	1.005	1.088	0.994	1.136	1.038
C1′–C2′	1.232	1.250	1.256	1.272	1.250	1.269	1.232	1.250
C1′–C6′	1.250	1.243	1.254	1.223	1.280	1.225	1.251	1.245
μ (a.u.)	0.9634	0.1727	1.3967	0.4433	2.0592	1.1405	0.0872	0.9538

planar structures. The torsional vibrational frequencies decrease with successive hydroxylation in the B-ring. These frequencies are 40 cm^{-1} in **1a**, 33 cm^{-1} in **2a**, 28 cm^{-1} in **3a**, and 37 cm^{-1} in **4a**.

We also examined the dipole moment μ in each species. As shown in Table 4, μ increases as the hydroxyl group is introduced into the B-ring. Moreover, μ values for the planar structures ***n*a** are larger than those for the non-planar structures ***n*b** in the case of $n=1$–3. According to Onsager's theory of the reaction field,[45] it is predicted that the planar structures (**1a**–**3a**) are stabilized more by the polar solvent effects than the non-planar structures (**1b**–**3b**). In the case of aurantinidin, μ in **4b** is greater than that in **4a** and this result is different from those in the other molecules.

3.2. Excited states

The SE–CI calculations were performed using the planar structures ***n*a** ($n=1$–4) optimized at the B3LYP/D95 level of theory. The results are shown in Table 5. The orbital energy diagrams near HOMO–LUMO and these MOs in **1a** are shown in Figures 4 and 5, respectively.

In all molecules **1a**–**4a**, the main configuration of the 2A′ state, which corresponds to the first excited state is the HOMO→LUMO excitation, as shown in Table 5. The main configuration of the 3A′ and 4A′ states, which correspond to the second and third excited states are the (HO−1)MO→LUMO and (HO−2)MO→LUMO excitations, respectively. The oscillator strength of the 2A′ state is large while those of the 3A′ and 4A′ states are very small. Therefore, it is predicted that λ_{max} observed in the spectral experiments originates in the 2A′ state.

We now discuss the excitation energies from the ground 1A′ state to the 2A′ state. The excitation energies to the 2A′ state are 3.58 eV in **1a**, 3.56 eV in **2a**, and 3.50 eV in **3a**. These energies decrease with the successive hydroxylations in the B-ring. On the other hand, the excitation energy in **4a** is 3.63 eV, which is greater than that in **1a**. Since this relative trend in the excitation energies is also obtained by calculations using the D95(d) basis set, it is indicated that the polarization function in the basis set have little effect on the results. This result, that is, successive hydroxylations in the B-ring cause a bathochromic shift in the λ_{max} while hydroxy substitution at the 6-position in the A-ring gives a hypsochromic shift, agrees with the experimental[1,9] and theoretical[25] results.

Since the main configuration of the lowest excited state is HOMO→LUMO excitation in all molecules, we notice the orbital energies in HOMO and LUMO. As shown in Figure 4, the HOMO–LUMO gap decreases with the

Table 5. Excited states of **1a**, **2a**, **3a**, and **4a** calculated by the SE–CI method

State	SE–CI/D95			SE–CI/D95(d)	Experimental λ_{max}[a,b]
	Main configuration ($\|C\|>0.2$)	Excitation energy[a]	Oscillator strength	Excitation energy[a]	
1a					
2A′	$0.96(12a''–13a'')$	3.58 (346)	1.2655	3.50 (354)	2.38 (520)
3A′	$0.87(11a''–13a'')-0.27(12a''–14a'')-0.21(10a''–13a'')$	4.83 (257)	0.0232	4.78 (259)	
4A′	$0.88(10a''–13a'')-0.24(10a''–14a'')+0.22(12a''–16a'')+0.20(11a''–13a'')$	4.94 (251)	0.0347	4.98 (249)	
2a					
2A′	$0.92(13a''–14a'')+0.27(12a''–14a'')$	3.56 (348)	1.2369	3.47 (357)	2.32 (535)
3A′	$0.90(12a''–14a'')-0.25(13a''–14a'')$	4.41 (281)	0.0171	4.46 (278)	
4A′	$0.90(11a''–14a'')+0.22(13a''–15a'')$	4.78 (259)	0.0203	4.74 (262)	
3a					
2A′	$0.93(14a''–15a'')$	3.50 (354)	1.2420	3.41 (363)	2.27 (546)
3A′	$0.93(13a''–15a'')-0.20(13a''–16a'')$	4.24 (293)	0.0418	4.27 (290)	
4A′	$0.88(12a''–15a'')+0.24(14a''–16a'')-0.23(11a''–15a'')$	4.69 (264)	0.0181	4.65 (266)	
4a					
2A′	$0.95(13a''–14a'')$	3.63 (341)	1.2883	3.55 (350)	2.48 (499)
3A′	$0.92(12a''–14a'')+0.21(12a''–15a'')$	4.46 (278)	0.0141	4.39 (283)	
4A′	$0.91(11a''–14a'')-0.25(11a''–15a'')$	4.91 (252)	0.0354	4.97 (250)	

[a] In eV (nm).
[b] Refs. 1,9 (methanol–HCl).

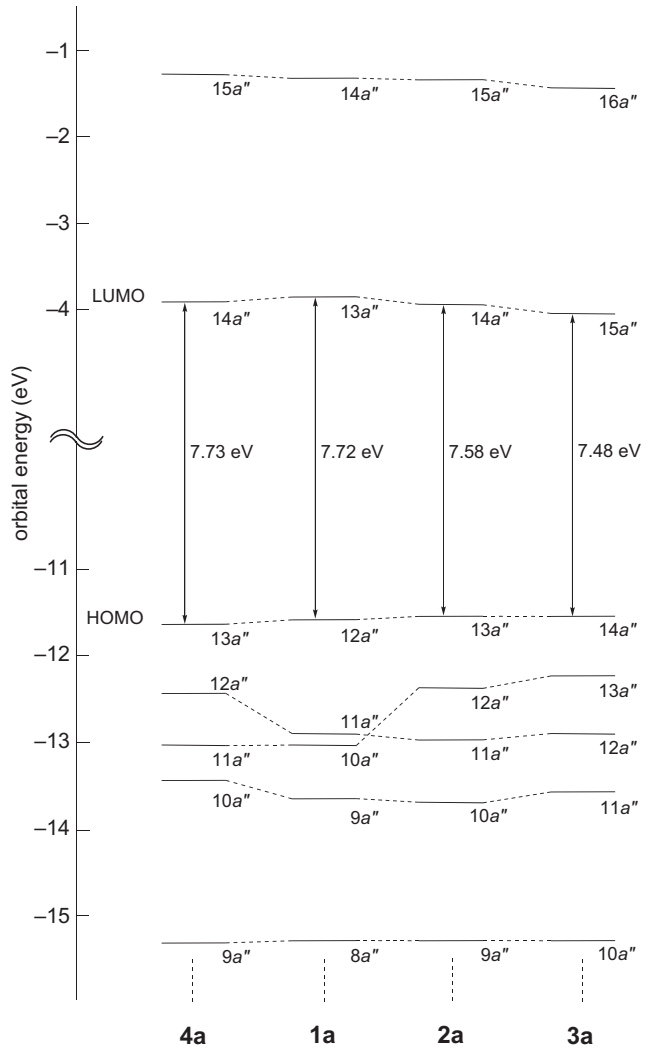

Figure 4. MO energy diagram at the RHF/D95//B3LYP/D95 level.

successive introduction of hydroxyl group in the B-ring (**1a**→**2a**→**3a**). These results correspond to the excitation energies in the SE–CI calculations and previous Hückel calculations.[18] The change in the HOMO–LUMO gap depends mainly on the lowering of the orbital energy in LUMO. On the other hand, the HOMO–LUMO gap in **4a** increases because the lowering of the HOMO energy level is greater than that of the LUMO energy level. In the next section, the variations of the HOMO and LUMO are discussed in terms of the orbital interactions.

As shown in Figure 5, the amplitude of the (HO−2)MO ($10a''$) in **1a** is localized in the B-ring, which originates in the e_{1g} orbital in benzene. The orbitals in **2a** and **3a**, which correspond to the $10a''$ orbital in **1a** are (HO−1)MOs ($12a''$ and $13a''$) and these orbital energies are higher than that of the $10a''$ orbital in **1a**. On the other hand, the (HO−2)MOs in **2a** and **3a**, which correspond to the $11a''$ orbital in **1a** have the same energy levels since these orbitals have large amplitudes in the A-ring part. This result shows that the second excited states in **2a** and **3a** correspond to the $4A'$ state in **1a** while the third excited state in **2a** and **3a** corresponds to the $3A'$ state in **1a**. In the case of **4a**, the (HO−1)MO is destabilized while

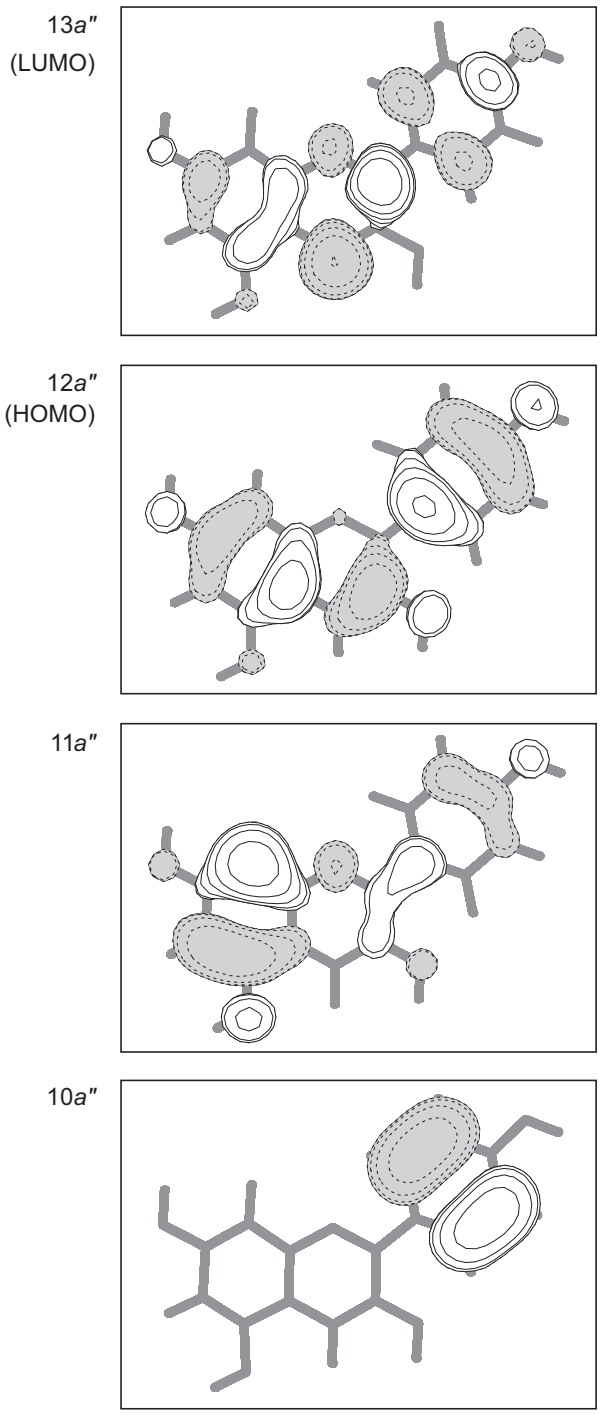

Figure 5. MO contours of **1a** at the RHF/D95//B3LYP/D95 level. MOLDEN[48] program was used for MO visualization.

the stability of the (HO−2)MO in **4a** is not changed in comparison with the orbital energies in **1a**.

We also investigated the strength of the C1′–C2 bond to predict the stable structures in the excited states. The Mayer bond orders at the RHF and SE–CI levels are shown in Table 6. One-particle density matrices are used for calculations at the SE–CI level. The main configuration of the $2A'$ state is excitation from the HOMO to the LUMO. In the HOMO, the C1′–C2 bond has an out-of-phase overlap. On the other hand, the amplitude of the C1′ atom is very

Table 6. Bond order $I(C1'–C2')$ and dipole moments μ

	$I(C1'–C2')$ [a]	μ (a.u.)[a]	μ (a.u.)[b]
1a			
$1A'$	1.044	1.2529	1.2116
$2A'$	1.065	0.9023	0.7561
$3A'$	0.996	2.9368	3.2589
$4A'$	1.091	2.8550	3.1299
2a			
$1A'$	1.003	1.8930	1.8228
$2A'$	1.044	1.4127	1.1036
$3A'$	1.051	3.0089	2.2621
$4A'$	0.977	2.8445	2.3287
3a			
$1A'$	0.985	2.7311	2.6441
$2A'$	1.031	1.9751	1.3352
$3A'$	1.041	2.5726	2.8765
$4A'$	0.949	3.9258	3.9018
4a			
$1A'$	1.043	0.2711	0.2566
$2A'$	1.063	0.4989	0.7143
$3A'$	0.997	4.0211	4.6228
$4A'$	1.092	3.8666	4.1052

[a] RHF/D95 level for the ground $1A'$ state and SE–CI level for the excited states.
[b] SAC level for the ground $1A'$ state and SAC-CI level for the excited states.

small, and therefore the bond overlap is too small in the LUMO. As a result, the bond order increases slightly in all molecules. This indicates that this bond is slightly strengthened by excitation to the $2A'$ state.

3.3. Orbital interactions in HOMO and LUMO

The variations of the HOMO and LUMO by the hydroxylation in the B-ring were examined in terms of the orbital interactions using the fragment molecular orbital (FMO) scheme.[46] At the σ-bond, which connects the B-ring with the C-ring, pelargonidin **1a** was divided into the benzopyrylium cation radical (A) and the phenol radical (B) and each fragment π-MO ($\psi^{A}_{la''}$, $\psi^{B}_{ma''}$) was calculated at the ROHF/D95 level of theory. Then the HOMO and LUMO in **1a** were represented by the linear combination of the obtained fragment π-MOs:

$$\psi_{HOMO} \cong +0.129\psi^{A}_{6a''} + 0.274\psi^{A}_{7a''} + 0.617\psi^{A}_{8a''} - 0.234\psi^{A}_{9a''} - 0.710\psi^{B}_{4a''},$$

$$\psi_{LUMO} \cong -0.901\psi^{A}_{9a''} + 0.179\psi^{B}_{2a''} + 0.422\psi^{B}_{4a''} - 0.239\psi^{B}_{6a''}.$$

Each fragment π-MO and the orbital interaction diagram are shown in Figure 6. In the HOMO, the linkage π-overlap population is -0.0180 and the major components of the population are the negative population between the $\psi^{A}_{8a''}$ and $\psi^{B}_{4a''}$ orbitals (-0.0206) and the positive population between the $\psi^{A}_{9a''}$ and $\psi^{B}_{4a''}$ orbitals ($+0.0197$). On the other hand, the major components of the overlap population in the LUMO (-0.0098) are the negative population between the $\psi^{A}_{9a''}$ and $\psi^{B}_{4a''}$ orbitals (-0.0451) and the positive population between the $\psi^{A}_{9a''}$ and $\psi^{B}_{6a''}$ orbitals ($+0.0569$).

The HOMO and LUMO at cyanidin **2a** and delphinidin **3a** were also examined by the same method. In the overlap populations in the HOMOs, the negative components, which correspond to that between the $\psi^{A}_{8a''}$ and $\psi^{B}_{4a''}$ orbitals in **1a** are -0.0153 (**2a**) and -0.0162 (**3a**). This out-of-phase overlap is weakened by the introduction of the *meta*-OH groups. The positive components ($\psi^{A}_{9a''} - \psi^{B}_{4a''}$ in **1a**) are $+0.0153$ (**2a**) and $+0.0169$ (**3a**), and so that the in-phase overlap is also weakened. For the introduction of the *meta*-OH groups, it is found that the variations of these two major components have the opposite effects on the stability of the HOMO. In the overlap populations in the LUMOs, the negative components ($\psi^{A}_{9a''} - \psi^{B}_{4a''}$ in **1a**) are -0.0392 (**2a**) and -0.0334 (**3a**) and the positive components ($\psi^{A}_{9a''} - \psi^{B}_{6a''}$ in **1a**) are $+0.0593$ (**2a**) and $+0.0636$ (**3a**). In the LUMO, the out-of-phase overlap is weakened while the in-phase overlap is strengthened. Both the components contribute to the stabilization in the LUMO. Here the AO coefficients at $C1'$ atom are not zero in the B-fragment MOs in **2a**, which correspond to the $\psi^{B}_{3a''}$ and $\psi^{B}_{5a''}$ orbitals in **1a**, because these orbitals are mixed with those, which correspond to the $\psi^{B}_{4a''}$ and $\psi^{B}_{6a''}$ orbitals in **1a**, respectively. Then, the negative overlap component in **2a** ($\psi^{A}_{9a''} - \psi^{B}_{4a''}$ in **1a**) is regarded as the sum of the overlap populations ($\psi^{A}_{6a''} - \psi^{B}_{3a''}$ and $\psi^{A}_{9a''} - \psi^{B}_{4a''}$ in **1a**). In the same way, the overlap population in **2a** ($\psi^{A}_{9a''} - \psi^{B}_{6a''}$ in **1a**) is also regarded as the sum of the overlap populations ($\psi^{A}_{9a''} - \psi^{B}_{5a''}$ and $\psi^{A}_{9a''} - \psi^{B}_{6a''}$ in **1a**).

Thus, we obtain the following qualitative explanation for the effects of the *meta*-OH groups. When the OH group is introduced into the *meta*-position at phenol part (B), the AO coefficients at $C1'$ atom decrease in the $\psi^{B}_{4a''}$ orbital while these increase in the $\psi^{B}_{6a''}$ orbital by the electron-withdrawing effect of the *meta*-OH group. Then, in the HOMO the out-of-phase overlaps between the fragment occupied MOs ($\psi^{A}_{6a''}$, $\psi^{A}_{7a''}$, and $\psi^{A}_{8a''}$) and the $\psi^{B}_{4a''}$ orbital is weakened and the in-phase overlap between the $\psi^{A}_{9a''}$ and $\psi^{B}_{4a''}$ orbitals is also weakened. As the result of the balance between these antithetic effects, the HOMO is destabilized. On the other hand, in the LUMO the out-of-phase overlap between the $\psi^{A}_{9a''}$ and $\psi^{B}_{4a''}$ orbitals is weakened and the in-phase overlap between $\psi^{A}_{9a''}$ and $\psi^{B}_{6a''}$ is strengthened, so that the LUMO is stabilized.

3.4. Excitation energies by the SAC/SAC-CI method

The low-excited states of **1a**–**4a** by the SAC/SAC-CI calculations are shown in Table 7. In all molecules, the main configurations of each electronic state by the SAC-CI calculations are consistent with the results of the SE–CI calculations. Thus, the main configurations of the $2A'$, $3A'$, and $4A'$ states are the HOMO→LUMO excitation, the (HO−1)MO→LUMO excitation, and the (HO−2)MO→LUMO excitation, respectively. The oscillator strength of the $2A'$ state is large while the strengths of the other states are very small. Moreover, the excitation energy within the visible region is only the $2A'$ state.

The excitation energies from the ground $1A'$ state to the $2A'$ state are 2.58, 2.56, 2.46, and 2.63 eV in **1a**, **2a**, **3a**, and **4a**, respectively. As shown in Table 1, experimental λ_{max} values observed in methanol–HCl solution are 2.38 eV (520 nm) in pelargonidin, 2.32 eV (535 nm) in cyanidin, 2.27 eV (546 nm) in delphinidin, and 2.48 eV (499 nm) in

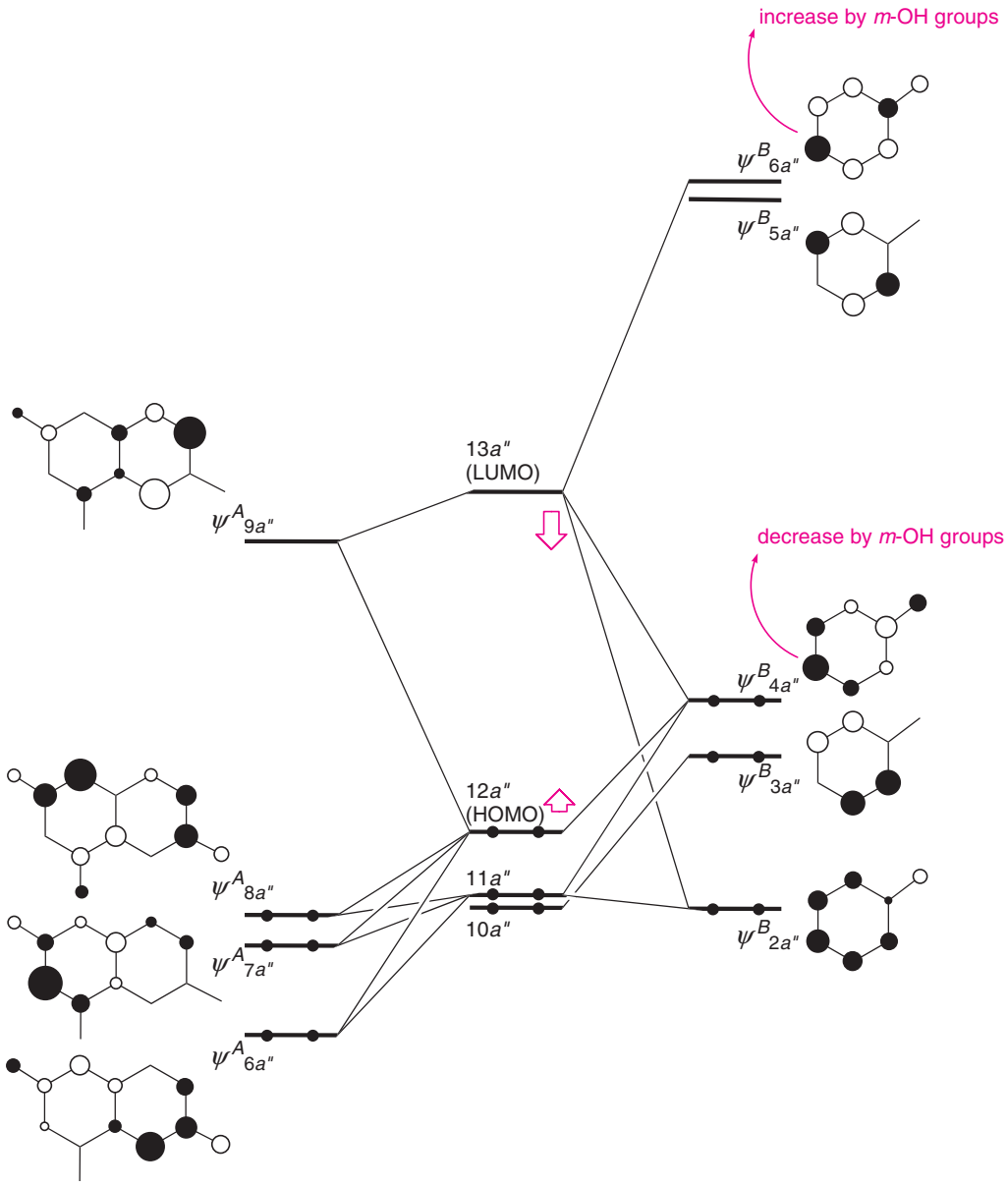

Figure 6. Fragment MO patterns and the orbital interaction diagram in **1a**.

aurantinidin. The SAC/SAC-CI results are better than the SE–CI results and the differences between the experimental λ_{max} and calculated energies are about 0.2 eV. Moreover, the results of these high-level ab initio calculations also show the same tendency as the SE–CI results, in that the lowest excitation ($1A' \rightarrow 2A'$) energy becomes bathochromic with successive hydroxylation in the B-ring while the excitation energy becomes hypsochromic with the 6-OH substitution.

Finally, the dipole moment μ in each electronic state is examined. The μ values calculated by the RHF/SE–CI and SAC/SAC-CI methods are shown in Table 6. In the ground $1A'$ state, the μ values calculated at the B3LYP level are different from the results at the RHF and SAC levels, but the difference between the SE–CI results and SAC-CI results is small. In **1a**, **2a**, and **3a**, the μ values in the $2A'$ state are smaller than those in the $1A'$ state while those in the $3A'$ and $4A'$ states are larger. In the case of **4a**, the μ value in the $1A'$ state is smaller than those in the $1A'$ state of the other molecules and the μ values in the $3A'$ and $4A'$ states are greater than those of the other molecules. According to Onsager's theory of the reaction field, it is predicted that the spectral shift of the $2A'$ state due to the polar solvent is small.

4. Conclusion

Using quantum chemical calculations, we investigated the structural stabilities and electronic structures of four anthocyanidin cationic molecules: pelargonidin, cyanidin, delphinidin, and aurantinidin. First, the stable structures in these molecules were examined at the B3LYP/D95 level of theory. Two stable structures, the planar structure and the non-planar structure, were obtained for each molecule. For all molecules, the planar structures are slightly more stable than the non-planar structures. Next, SE–CI and SAC/SAC-CI calculations were carried out for the planar structures in

Table 7. Excited states of **1a**, **2a**, **3a**, and **4a** calculated by the SAC/SAC-CI method

States	Main configuration ($\|C\|>0.1$)	Excitation energy[a]	Oscillator strength	Experimental λ_{max}[a,b]
1a				
2A′	$0.94(12a''–13a'')-0.12(11a''–13a'')-0.10(12a'',9a''–13a'',13a'')$	2.58 (481)	0.7823	2.38 (520)
3A′	$0.91(11a''–13a'')-0.15(10a''–13a'')-0.12(9a''–13a'')-0.11(12a''–14a'')+0.10(12a''–13a'')$	3.48 (356)	0.0311	
4A′	$0.89\ (10a''–13a'')+0.20(12a''–16a'')+0.15(11a''–13a'')-0.14(10a''–14a'')-0.16(12a'',10a''–13a'',13a'')$	3.89 (319)	0.0159	
2a				
2A′	$0.93(13a''–14a'')+0.16(12a''–14a'')-0.12(11a''–14a'')$	2.56 (484)	0.7211	2.32 (535)
3A′	$0.92(12a''–14a'')-0.16(13a''–14a'')-0.13(11a''–14a'')$	3.19 (388)	0.0121	
4A′	$0.91(11a''–14a'')+0.14(12a''–14a'')-0.12(10a''–14a'')+0.11(12a''–15a'')$	3.56 (348)	0.0482	
3a				
2A′	$0.94(14a''–15a'')+0.12(12a''–15a'')-0.10(13a''–15a'')-0.11(12a'',14a''–15a'',15a'')$	2.46 (504)	0.7339	2.27 (546)
3A′	$0.93(13a''–15a'')+0.12(14a''–18a'')-0.10(13a''–16a'')+0.14(13a'',14a''–15a'',15a'')$	2.99 (414)	0.0119	
4A′	$-0.92(12a''–15a'')+0.17(11a''–15a'')+0.11(14a''–15a'')$	3.36 (369)	0.0057	
4a				
2A′	$0.95(13a''–14a'')-0.15(10a'',13a''–14a'',14a'')$	2.63 (472)	0.8068	2.48 (499)
3A′	$0.94(12a''–14a'')+0.10(12a''–15a'')$	3.01 (412)	0.0156	
4A′	$0.91(11a''–14a'')-0.16(13a''–17a'')-0.16(11a''–15a'')+0.11(13a''–16a'')-0.16(11a'',13a''–14a'',14a'')$	3.87 (321)	0.0169	

[a] In eV (nm).
[b] Refs. 1,9 (methanol–HCl).

all molecules. These high-level ab initio calculations have shown that the lowest excitation energies, which correspond to the visible absorption maxima in the spectral experiments vary according to the existence of hydroxyl groups without taking solvent effects into account. Thus, hydroxy substitution at the 6-position in the A-ring increases the lowest excitation energy while successive hydroxylations in the B-ring decrease the excitation energies.

Now we examine the electronic excited states in not only the anthocyanidin cationic form but also neutral and anionic forms by the TD-DFT method with larger basis sets, including the PCM theory.[47]

References and notes

1. Harborne, J. B. *Comparative Biochemistry of the Flavonoids*; Academic Press: New York, 1967.
2. Goodwin, T. W., Ed. *Chemistry and Biochemistry of Plant Pigments*; 2nd ed.; Academic: New York, 1990; Vols. 1,2.
3. Goodwin, T.W., Ed.; *Plant Pigments*; Academic: New York, 1990.
4. Goto, T.; Kondo, T. *Angew. Chem., Int. Ed. Engl.* **1991**, *30*, 17.
5. Brouillard, R.; Dangles, O. In *The Flavonoids*; Harborne, J. B., Ed.; Chapman and Hall: London, 1994; p 565.
6. Brouillard, R. In *Anthocyanins as Food Colors*; Markakis, P., Ed.; Academic: New York, 1982.
7. Hayashi, K. In *The Chemistry of Flavonoid Compounds*; Geissman, T. A., Ed.; Pergamon: Oxford, 1962; p 248.
8. Schou, S. A. *Helv. Chim. Acta* **1927**, *10*, 907.
9. Harborne, J. B. *Biochem. J.* **1958**, *70*, 22.
10. Asen, S.; Stewart, R. N.; Norris, K. H. *Phytochemistry* **1972**, *11*, 1139.
11. Robinson, M. G.; Robinson, R. *Biochem. J.* **1931**, *25*, 1687.
12. Saito, N.; Osawa, Y.; Hayashi, K. *Phytochemistry* **1971**, *10*, 445.
13. Honda, T.; Saito, N. *Heterocycles* **2002**, *56*, 633.
14. Shibata, K.; Shibata, Y.; Kasiwagi, I. *J. Am. Chem. Soc.* **1919**, *41*, 208.
15. Kondo, T.; Yoshida, K.; Nakagawa, A.; Kawai, T.; Tamura, H.; Goto, T. *Nature* **1992**, *358*, 515.
16. Shiono, M.; Matsugaki, N.; Takeda, K. *Nature* **2005**, *436*, 791.
17. Pauling, L. In *Progress in the Chemistry of Organic Natural Products*; Zechmeister, L. Ed.; Springer: Wien, 1939; Vol. 3.
18. Bendz, G.; Mårtensson, O.; Nilsson, E. *Ark. Kemi* **1967**, *27*, 65.
19. Kurtin, W. E.; Song, P.-S. *Tetrahedron* **1968**, *24*, 2255.
20. Song, P.-S.; Moore, T. A.; Sun, M. In *The Chemistry of Plant Pigments*; Chichester, C. O., Ed.; Academic: New York, 1972.
21. Rastelli, G.; Costantino, L.; Albasini, A. *J. Mol. Struct. (Theochem)* **1993**, *279*, 157.
22. Pereira, G. K.; Donate, P. M.; Galembeck, S. E. *J. Mol. Struct. (Theochem)* **1996**, *363*, 87.
23. Pereira, G. K.; Donate, P. M.; Galembeck, S. E. *J. Mol. Struct. (Theochem)* **1997**, *392*, 169.
24. Pereira, G. K.; Galembeck, S. E. *Spectrochim. Acta Part A* **1998**, *54*, 339.
25. Torskangerpoll, K.; Børve, K. J.; Andersen, Ø.M.; Sæthre, L. J. *Spectrochim. Acta Part A* **1999**, *55*, 761.
26. Merlin, J.-C.; Statoua, A.; Cornard, J.-P.; Saidi-Idrissi, M.; Brouillard, R. *Phytochemistry* **1994**, *35*, 227.
27. Figueiredo, P.; Elhabiri, M.; Toki, K.; Saito, N.; Dangles, O.; Brouillard, R. *Phytochemistry* **1995**, *41*, 301.
28. Figueiredo, P.; Elhabiri, M.; Saito, N.; Brouillard, R. *J. Am. Chem. Soc.* **1996**, *118*, 4788.
29. Becke, A. D. *J. Chem. Phys.* **1993**, *98*, 5648.
30. Lee, C.; Yang, W.; Parr, R. G. *Phys. Rev. B* **1988**, *37*, 785.
31. Dunning, T. H., Jr. *J. Chem. Phys.* **1970**, *53*, 2823.
32. Dunning, T. H., Jr.; Hay, P. J. In *Methods of Electronic Structure Theory*; Schaefer, H. F., III, Ed.; Plenum: New York, 1977.
33. Nakatsuji, H.; Hirao, K. *J. Chem. Phys.* **1978**, *68*, 2053.
34. Nakatsuji, H. *Chem. Phys. Lett.* **1978**, *59*, 362.
35. Nakatsuji, H. *Chem. Phys. Lett.* **1979**, *67*, 334.
36. Nakatsuji, H. In *Computational Chemistry*: *Reviews of Current Trends*; Leszczynski, J., Ed.; World Scientific: Singapore, 1997; Vol. 2.
37. Nakatsuji, H. *Chem. Phys.* **1983**, *75*, 425.
38. Nakatsuji, H.; Hasegawa, J.; Hada, M. *J. Chem. Phys.* **1996**, *104*, 2321.

39. Frisch, M. J.; Trucks, G. W.; Schlegel, H. B.; Scuseria, G. E.; Robb, M. A.; Cheeseman, J. R.; Montgomery, J. A., Jr.; Vreven, T.; Kudin, K. N.; Burant, J. C.; Millam, J. M.; Iyengar, S. S.; Tomasi, J.; Barone, V.; Mennucci, B.; Cossi, M.; Scalmani, G.; Rega, N.; Petersson, G. A.; Nakatsuji, H.; Hada, M.; Ehara, M.; Toyota, K.; Fukuda, R.; Hasegawa, J.; Ishida, M.; Nakajima, T.; Honda, Y.; Kitao, O.; Nakai, H.; Klene, M.; Li, X.; Knox, J. E.; Hratchian, H. P.; Cross, J. B.; Bakken, V.; Adamo, C.; Jaramillo, J.; Gomperts, R.; Stratmann, R. E.; Yazyev, O.; Austin, A. J.; Cammi, R.; Pomelli, C.; Ochterski, J. W.; Ayala, P. Y.; Morokuma, K.; Voth, G. A.; Salvador, P.; Dannenberg, J. J.; Zakrzewski, V. G.; Dapprich, S.; Daniels, A. D.; Strain, M. C.; Farkas, O.; Malick, D. K.; Rabuck, A. D.; Raghavachari, K.; Foresman, J. B.; Ortiz, J. V.; Cui, Q.; Baboul, A. G.; Clifford, S.; Cioslowski, J.; Stefanov, B. B.; Liu, G.; Liashenko, A.; Piskorz, P.; Komaromi, I.; Martin, R. L.; Fox, D. J.; Keith, T.; Al-Laham, M. A.; Peng, C. Y.; Nanayakkara, A.; Challacombe, M.; Gill, P. M. W.; Johnson, B.; Chen, W.; Wong, M. W.; Gonzalez, C.; Pople, J. A. *Gaussian 03, Revision C.02*; Gaussian, Inc.: Wallingford CT, 2004.
40. Schmidt, M. W.; Baldridge, K. K.; Boatz, J. A.; Elbert, S. T.; Gordon, M. S.; Jensen, J. J.; Koseki, S.; Matsunaga, N.; Nguyen, K. A.; Su, S. J.; Windus, T. L.; Dupuis, M.; Montgomery, J. A. *J. Comput. Chem.* **1993**, *14*, 1347.
41. Mulliken, R. S. *J. Chem. Phys.* **1955**, *23*, 1833.
42. Mayer, I. *Chem. Phys. Lett.* **1983**, *97*, 270.
43. Ueno, K.; Saito, N. *Acta Crystallogr., Sect. B* **1977**, *33*, 114.
44. Saito, N.; Ueno, K. *Heterocycles* **1985**, *23*, 2709.
45. Onsager, L. *J. Am. Chem. Soc.* **1936**, *58*, 1486.
46. Fujimoto, H.; Hoffmann, R. *J. Phys. Chem.* **1974**, *78*, 1167.
47. Sakata, K.; Saito, N.; Honda, T., to be submitted.
48. Schaftenaar, G. *MOLDEN*, QCPE Program No. 619, University of Indiana.